Zeolites Hot Paper

Deutsche Ausgabe: DOI: 10.1002/ange.201607800
Internationale Ausgabe: DOI: 10.1002/anie.201607800

Synthesis of a Ferrolite: A Zeolitic All-Iron Framework

*Allison M. Latshaw, W. Michael Chance, Gregory Morrison, Karl D. zur Loye, Branford O. Wilkins, Mark D. Smith, Pamela S. Whitfield, Melanie J. Kirkham, Sebastian A. Stoian, and Hans-Conrad zur Loye**

Abstract: *Crystals of the first sodalite-type zeolite containing an all-iron framework, a ferrolite, $Ba_8(Fe_{12}O_{24})Na_y(OH)_6{\cdot}x\,H_2O$, were synthesized using the hydroflux method in nearly quantitative yield. $Ba_8(Fe_{12}O_{24})Na_y(OH)_6{\cdot}x\,H_2O$ crystallizes in the cubic space group $Pm\bar{3}m$ with $a = 10.0476(1)$ Å. Slightly distorted FeO_4 tetrahedra are linked to form Fe_4O_4 and Fe_6O_6 rings, which in turn yield channels and internal cavities that are characteristic of the sodalite structure. Barium, sodium, and hydroxide ions and water molecules are found in the channels and provide charge balance. Magnetic measurements indicate that the ferrolite exhibits magnetic order up to at least 700 K, with the field-cooled and zero-field-cooled curves diverging. Analysis of the ^{57}Fe Mössbauer spectra revealed two spectral components that have equal spectral areas, indicating the presence of two subsets of iron centers in the structure. Dehydrated versions of the ferrolite were also prepared by heating the sample.*

Zeolites, a class of microporous, crystalline aluminosilicates, occur naturally but are also synthesized on an industrial scale to satisfy the widespread demand for their use in catalysis, adsorption, and ion exchange applications.[1–4] As a class, they can be described by the general formula $M_{2/n}O{\cdot}Al_2O_3{\cdot}y\,SiO_2{\cdot}x\,H_2O$, where n is the valence of the metal cation, and where y can range from 2 to over 200. To date, over 40 naturally occurring zeolites have been identified, and over 200 unique zeolite frameworks have been created in the laboratory. A traditional zeolite exhibits a three-dimensional framework structure comprising AlO_4 and SiO_4 tetrahedra connected via -Si-O-Al- linkages that yield porous structures with enclosed regular internal cavities and channels of discrete size and shape in which Group I and II cations reside and provide charge balance.[2]

Although zeolites were first discovered in 1756 by the Swedish mineralogist Cronstedt, it was not until the second half of the last century that synthetic analogues were created in laboratories. Moreover, the proliferation of new compositions led to the expansion of the traditional definition of zeolites to include non-aluminosilicate compositions.[2,5] In the 1980s, the incorporation of titanium, chromium, iron,[6] tin, gallium, germanium,[7] and other metals into aluminosilicate frameworks gave rise to the metallosilicate molecular sieves, which was soon thereafter followed by the discovery of the aluminophosphates (ALPOs). The incorporation of silica and metal ions into ALPOs yielded new classes of zeolites, that is, the silicoaluminophosphates (SAPOs) and the metalloaluminophosphates (MeAPOs). Other additions to this expansive family of materials include the octahedral–tetrahedral frameworks, the germanosilicates, and an ever-increasing variety of structures with ever-larger pore sizes.[8] The synthesis of these new materials has had a tremendous impact on the field of catalysis and molecular sieve applications. Throughout the history of zeolites, new synthetic methods and/or the incorporation of new elements have led to the discovery of new classes of molecular sieves with new applications. While transition-metal elements have been substituted into aluminosilicate frameworks, zeolites with frameworks consisting entirely of transition-metal cations have not yet been prepared. Herein, we present the first example of a ferrolite, a zeolite containing an all-iron framework, $Ba_8(Fe_{12}O_{24})Na_y(OH)_6{\cdot}x\,H_2O$ (refined to a composition of $Ba_8Fe_{12}H_6Na_{2.84}O_{36.34}$ by single crystal X-ray diffraction), that crystallizes in the sodalite structure.

The synthesis of this new material was enabled by our development of the hydroflux crystal growth technique, which occupies a niche area between hydrothermal synthesis and molten flux chemistry.[9–11] The new all-iron zeolite (ferrolite) was crystallized in a hydroflux reaction, where $Fe(NO_3)_3{\cdot}9\,H_2O$ (4.28 mmol), $Ba(OH)_2{\cdot}8\,H_2O$ (4.28 mmol), NaOH (9 g), and H_2O (7 g) were heated at 230 °C in a PTFE-lined stainless-steel autoclave for 24 hours followed by slow cooling at a rate of 0.3 °C min^{-1} to 80 °C. Block crystals measuring 0.05 to 0.1 mm in size with truncated corners were isolated in nearly quantitative yield by removing the residual flux with methanol under sonication.

The structure was determined by using a combination of single-crystal X-ray diffraction and powder neutron diffraction. $Ba_8(Fe_{12}O_{24})Na_y(OH)_6{\cdot}x\,H_2O$ crystallizes in the space

[*] Prof. Dr. H.-C. zur Loye
Chemistry and Biochemistry
University of South Carolina
Columbia, SC 29208 (USA)
E-mail: zurloye@mailbox.sc.edu
Dr. A. M. Latshaw, Dr. W. M. Chance, Dr. G. Morrison, K. D. zur Loye, B. O. Wilkins, M. D. Smith
Chemistry and Biochemistry
University of South Carolina
Columbia, SC 29208 (USA)
Dr. P. S. Whitfield, Dr. M. J. Kirkham
Oak Ridge National Laboratory
Oak Ridge, TN 37831 (USA)
Dr. S. A. Stoian
National High Magnetic Field Laboratory
Florida State University
Tallahassee, FL 32310 (USA)
Supporting information and the ORCID identification number(s) for the author(s) of this article can be found under: http://dx.doi.org/10.1002/anie.201607800.

group $Pm\bar{3}m$ with a cubic lattice parameter of $a = 10.0476(1)$ Å (see the Supporting Information, Tables S1–S3). The structure of the ferrolite is shown in Figure 1 (left), where it is compared with the structure of the cubic sodalite mineral $[Na_8[Al_6Si_6O_{24}]Cl_2]$ (right). As can be seen, the all-iron and silicon/aluminum frameworks are essentially identical.

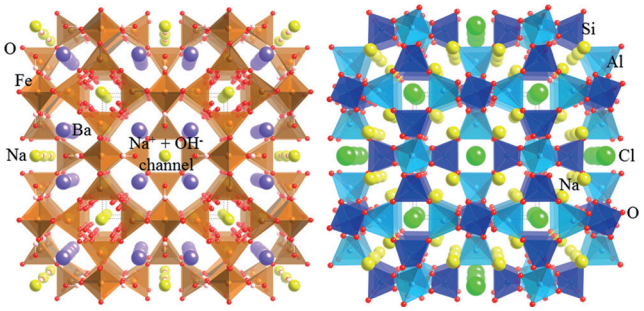

Figure 1. Left: $Ba_8(Fe_{12}O_{24})Na_y(OH)_6{\cdot}xH_2O$. Fe tetrahedra shown in orange, Na atoms in yellow, and Ba atoms in purple. Right: $Na_8(Al_6Si_6O_{24})Cl_2$. Al and Si tetrahedra shown in light blue and dark blue, respectively; Na atoms shown in yellow and Cl in green.

The iron ions are found in slightly irregular FeO_4 tetrahedra with bond lengths of 1.7883(9) Å (Fe–O1) and 1.8458(10) Å (Fe–O2; dehydrated: 1.785(3) Å (Fe–O1) and 1.8477(14) Å (Fe–O2)). Each FeO_4 tetrahedron is connected to four other tetrahedra, creating planar Fe_4O_4 rings and puckered Fe_6O_6 rings in the process. The $Fe_{12}O_{24}$ sodalite units are linked via shared Fe_4O_4 rings to form the extended sodalite structure (Figure 2). The channels that form are occupied by sodium and barium as well as hydroxide ions and water (not shown).

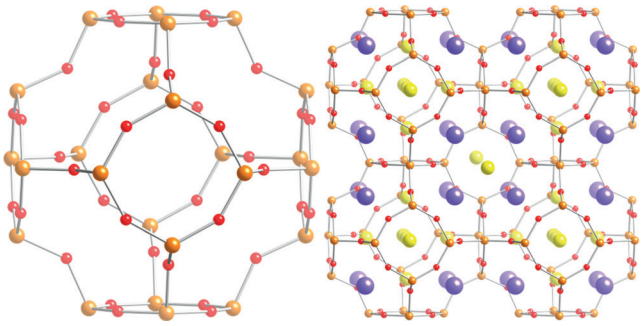

Figure 2. Left: The Fe–O sodalite cage (Fe orange, O red). Right: The extended sodalite framework including the location of the Na (yellow) and Ba cations (purple).

The as-synthesized ferrolite crystals contain disordered water molecules, some disordered sodium cations (Na2), and likely hydroxide ions in the central cavity, making it challenging to obtain a firm stoichiometry. Whereas for the $Fe_{12}O_{24}$ sodalite unit, the Ba and Na1 cations are readily refined and located, the water and Na2 species are found in the central cavity (Figure 3). TGA data (Figure 4a) demonstrate that it is possible to remove water from the central

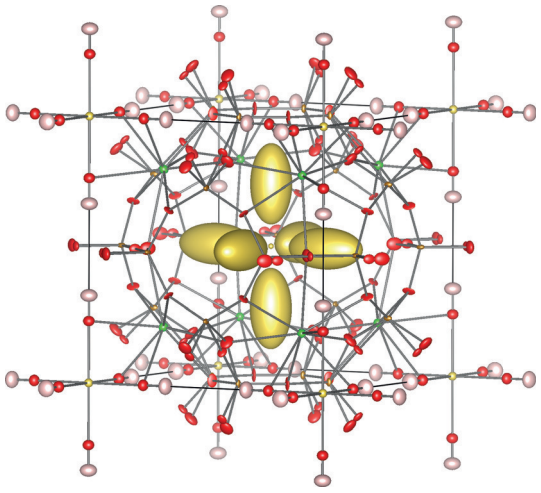

Figure 3. Rietveld structure from the refinement of neutron data showing the arrangement of the Na cations (yellow) and hydroxide ions in the inner cage structure.

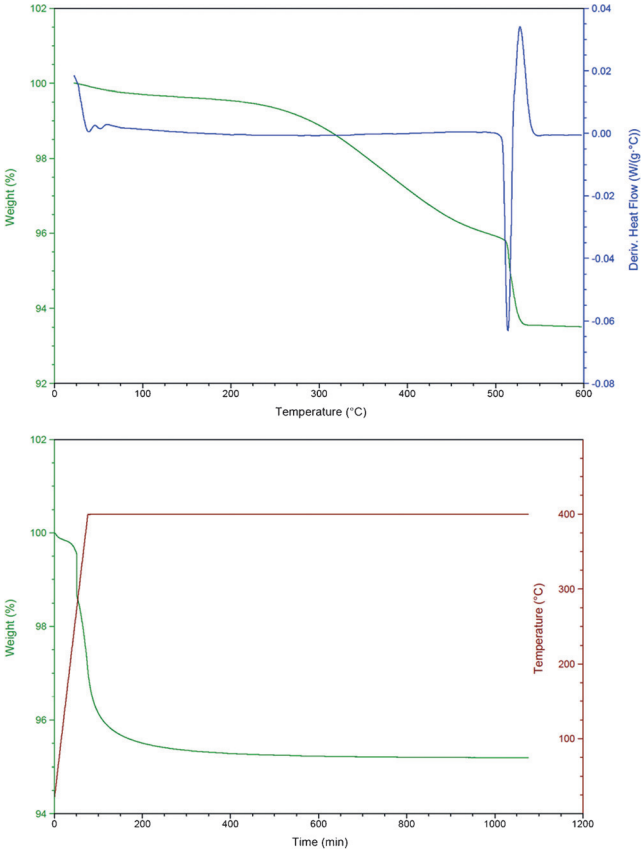

Figure 4. Top: TGA data showing that the framework decomposes just above 500 °C. Bottom: The dehydrated material can be prepared by isothermal heating at 400 °C overnight.

cavity. As the sample is heated, water continues to be lost until the ferrolite thermally decomposes at just above 500 °C, as confirmed by powder X-ray diffraction. Essentially all of the water can be removed by heating the ferrolite at 400 °C for extended periods of time (Figure 4b), to obtain a dehydrated

composition. Once this is achieved, the X-ray structure solution improves significantly as less electron density occupies the channels and central cavities (see Tables S4 and S5). To assist in assigning the electron density, ICP-OES elemental analysis was carried out on these zeolites. Thus a batch of ground crystals gave an average composition of $Na_{3.165}Ba_{7.955}Fe_{12}O_x$. One sodium cation (Na1) is crystallographically ordered, leaving 2.16 sodium cations for the central cavity. The crystallographically determined composition of $Na_{2.84}Ba_8Fe_{12}O_{24}(OH)_6(OH^-/H_2O)_{6.3}$ is in reasonably good agreement with the ICP-OES data, the main discrepancy arising from the concentration of the disordered sodium ions in the channel. More importantly, however, it confirms the crystallographically well-defined framework composition. As expected for a rigid framework structure, the lattice parameter of the dehydrated zeolite, $a = 10.0275(3)$ Å, is very similar to that of the hydrated version ($a = 10.0476(1)$ Å).

To obtain a better understanding of the crystal structure and to explore the existence of potential low-temperature phase transitions, variable-temperature powder neutron diffraction experiments were carried out at the POWGEN beamline at the Spallation Neutron Source at Oak Ridge National Laboratory. The Rietveld refinement of the 300 K dehydrated and magnetically ordered ferrolite data set is shown in Figure 5. The stoichiometry was refined to

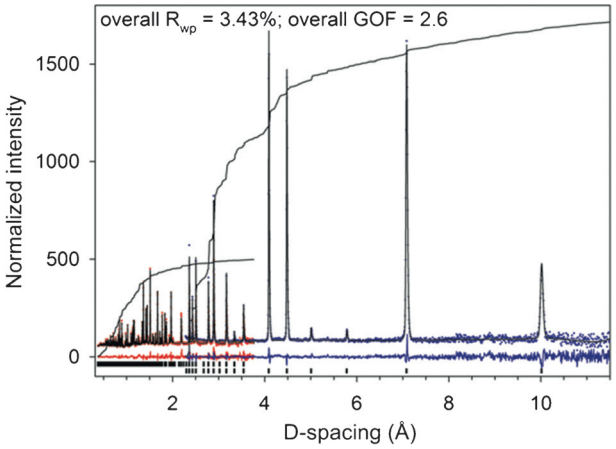

Figure 5. Rietveld refinement of merged neutron diffraction data from frames 2 and 4 for the dehydrated ferrolite measured at 300 K.

$Na_{3.6(3)}Ba_8Fe_{12}O_{24}(OH)_6$, which is in reasonable agreement with the ICP and X-ray stoichiometries. Although not done in the final model, constraining the Na content to the value from the ICP data did not significantly degrade the fit. The displacement of the disordered Na3 ions was very large, indicating significant mobility within the channels. Other than the expected temperature-induced contraction of the *a* lattice parameter, the structure remains unchanged upon cooling to 10 K.

Based on the refined composition of $Na_{2.84}Ba_8Fe_{12}O_{24}(OH)_6(OH^-/H_2O)_{6.3}$, we conclude that the average oxidation state of iron is very close to 3.0 (2.93), which indicates that the framework is built from Fe^{III}-based FeO_4 tetrahedra. Tetrahedral high-spin ferric ions have a d^5 electron configuration, making this framework very rich in unpaired electrons. To investigate the magnetic behavior of $Na_{2.84}Ba_8Fe_{12}O_{24}(OH)_6(OH^-/H_2O)_{6.3}$, both zero field cooled (ZFC) and field cooled (FC) magnetic susceptibility data were collected. Figure 6 shows the temperature dependence of the magnetic data and reveals that the ZFC and FC traces do not overlap. Interestingly, even at temperatures as high as 700 K, the observed behavior clearly deviates from the Curie–Weiss law. As the material is not thermally stable at higher temperatures, we were unable to pursue magnetic measurements at temperatures higher than 700 K.

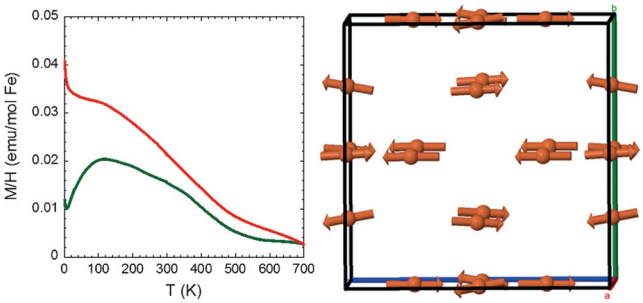

Figure 6. Left: ZFC and FC data collected at 1000 Oe. Right: The arrangement of the iron spins in the ferrolite, resulting in canted antiferromagnetic behavior.

The large iron content of ferrolite provides us with the opportunity to further investigate the electronic structure of the iron sites by ^{57}Fe Mössbauer spectroscopy. Figure 7 shows a series of temperature- and field-dependent spectra recorded for a ground powder sample of the zeolite. The zero-field spectra feature a six-line pattern, which demonstrates the presence of a spontaneous magnetic field that acts on the ^{57}Fe nuclei.[12] In turn, this observation reveals the presence of a magnetically ordered ground state. Interestingly, ordering is preserved even at room temperature. However, as the temperature is increased above 100 K, an additional two-line component, that is, a quadrupole doublet, is observed. This finding suggests that some particles present in the powder sample are nanosized and that they exhibit typical superparamagnetic behavior. The solid gray traces superimposed on the experimental data are spectral simulations obtained from the sum of two components for the field-dependent 4.2 K spectra and three components for the zero-field, temperature-dependent spectra, respectively. The individual components are drawn separately above the experimental spectra, and the parameters derived from these simulations are listed in Table S7.[13] The observation of distinct spectral components that exhibit magnetic hyperfine splitting reveals the presence of multiple magnetic sublattices.

The two sextets have equal intensities and are essentially identical but differ from one another in terms of the sign of the component of the electric field gradient (EFG) tensor that is found along the spontaneous fields, ε (Figure 7).[14] Moreover, all three subspectra are characterized by isomer shifts, $\delta = 0.28$–0.35 mm s^{-1}, that are typical of high-spin ferric ions supported by an all-oxygen tetracoordinate environment. The magnitude of the internal field associated with the observed

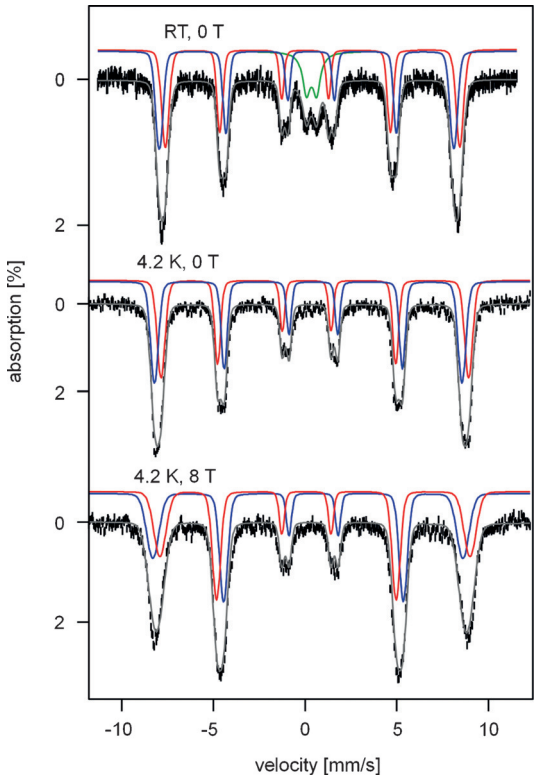

Figure 7. Selected ^{57}Fe Mössbauer spectra recorded for the Na-containing zeolite sample. The solid gray traces superimposed on the experimental spectra are simulations obtained from the sum of two/three components that are drawn above the spectra (see Table S7).

magnetic hyperfine splitting of the two sextets, $B_{int} \approx 52(1)$ T, is also typical of $S = 5/2$ Fe^{III} ions and is essentially identical to that observed for the iron(III) sites of binary iron oxides. The observation of two spectral components that exhibit magnetic hyperfine splitting and have equal areas is consistent with the presence of an antiferromagnetically ordered state.[15,16]

To assess the nature of the exchange interactions of the two magnetic sublattices, we performed a series of field-dependent measurements. In zero field, the two sextets exhibit an approximate 3:2:1:1:2:3 pattern, which demonstrates that the hyperfine fields are randomly distributed with respect to the propagation direction of the 14.41 keV γ-ray used to detect the Mössbauer effect. In our measurements, the magnetic field was applied parallel to the propagation direction of the γ-ray. For a collinear antiferromagnet, we expect the internal field to align parallel to the applied field. Consequently, for a setup such as ours, we expect the applied field to induce a decrease in the intensities of the central, $\Delta m_I = 0$ lines. In contrast, Figures 7 and S1 reveal a field-induced increase in the intensities of the $\Delta m_I = 0$ lines. This demonstrates an orthogonal alignment of the internal field with respect to the field, which in turn establishes that the moments associated with the two individual magnetic sublattices are canted, that is, they are found in a non-colinear antiferromagnetically ordered state.[17] Interestingly, the observation of a single quadrupole doublet at room temperature strongly suggests that the iron sites of the two magnetic sublattices have not only identical isomer shifts but also identical quadrupole splittings. Consequently, the observation of dissimilar ε values for the two magnetic subspectra does not necessarily indicate that the EFG tensors are different but rather that the local magnetic moments of the iron sites sample different directions (components) of the EFG tensor, and thus further corroborates the presence of canting (Figure S2). The magnetic neutron structure could be refined equally well in either the magnetic space group $P4'$ or $\bar{P}4'$; both represent a canted antiferromagnetic arrangement, consistent with the Mössbauer and magnetic susceptibility data (Figures 6 and S3).

The nuclear structure was refined as cubic $Pm\bar{3}m$ for consistency with the single-crystal structure determination. The magnetic structure was refined with a lower symmetry with the required linking of certain parameters between the structures (e.g., unit-cell parameters, unit-cell volumes, iron site positions). Magnetic lattices may or may not have the same symmetry as the nuclear structure (equivalent to the parent paramagnetic structure) in a material. Incommensurate magnetic structures exhibit the latter feature by definition but differing symmetries may also occur in commensurate magnetic structures. For example, the magnetic lattice in magnetite (Fe_3O_4) is rhombohedral with three distinct iron sites while the nuclear structure is a cubic spinel with only two distinct iron sites. The relationship between the magnetic and parent structure may be tackled in different ways, including describing the complete structure in a single magnetic Shubnikov group, by using basis vectors, or by separating the nuclear and magnetic contributions to the diffraction pattern into two distinct "phases". This study used the last approach owing to the increased flexibility afforded by decoupling the nuclear and magnetic contributions.

Historically, the expansion of the field of zeolites occurred by new synthetic routes that enabled the preparation of new framework types, such as the use of templating agents, which led to the famous ZSM-5 zeolite by Mobil,[23] at the time a game changer in the field of catalysis. Furthermore, the extensive history of zeolites makes it clear that from a single starting point, an entirely new structural family can be created, as Edith Flanigen did at Union Carbide when she created the AlPOs. Hence, the synthesis of this new all-iron zeolite can become the seed for future research with potential impact on a large number of research areas. This structure as well as conceivable additional structure types may well impact the field of catalysis; the presence of iron cations with their unpaired electrons may promote research into new magnetic materials, and the iron combined with the presence of sodium in the channels is likely of interest to researchers in the field of sodium-ion batteries for stationary power storage. Work is underway to chemically modify the composition of this ferrolite as well as to create ferrolites that crystallize in other framework structure types.

Experimental Section

Crystals of both the unheated (original growth from hydroflux) and heated compounds were transparent brown cubes. X-ray intensity data measurements were made using a Bruker D8 QUEST diffractometer equipped with a PHOTON 100 CMOS area detector and an

Incoatec microfocus source (Mo Kα radiation, $\lambda = 0.71073$ Å).[18] All of many crystals surveyed indexed to a primitive cubic unit cell with $a \approx 10.0$ Å. All data collections covered 100% of the reciprocal space to a minimum $2\theta_{max} = 65°$, with high average reflection redundancies (> 13). Raw area detector data frames were reduced and corrected for absorption effects using the SAINT+ and SADABS programs.[18] Final unit-cell parameters were determined by least-squares refinement of large sets of strong reflections ($I > 10\sigma(I)$) taken from each data set. An initial structural model was obtained with SHELXS using direct methods.[19] Subsequent difference Fourier calculations and full-matrix least-squares refinement against F^2 were performed with SHELXL-2014[19] using the ShelXle interface.[20]

The magnetic susceptibility of the zeolite was measured using a Quantum Design MPMS3 SQUID magnetometer equipped with an oven attachment. A ground sample of 4.58 mg was loaded into a pouch made of silver foil, which was then crimped shut. For low-temperature measurements, the pouch was mounted onto a quartz paddle using GE-7031 varnish. For high-temperature measurements, the pouch was embedded in ZIRCAR cement and mounted onto an oven stick. The zero-field-cooled and field-cooled cooling magnetic susceptibilities were measured as a function of temperature between 2 and 700 K at an applied field of 1000 Oe. The sample was removed from the magnetometer to change mounts at 300 K. The magnetization as a function of field was collected at 2 K prior to heating in the oven attachment. For all measurements, the measured magnetic moment was corrected for the diamagnetic contribution of the silver pouch.

The samples investigated by Mössbauer spectroscopy contained 10–30 mg of finely ground powder dispersed in an inert eicosane matrix. The spectrometer was operated in a constant acceleration mode, used a ca. 100 mCi 57Co(Rh) source, and allowed for applied fields parallel to the observed γ-radiation. Field- and temperature-dependent spectra were recorded using a Mössbauer spectrometer equipped with a Janis 8DT Super Varitemp cryostat that was outfitted with an 8 T superconducting magnet. Isomer shifts are quoted against the centroid of a room-temperature spectrum recorded for a standard iron metal foil. Mössbauer spectral simulations were performed using the WMOSS software (See Co., formerly WEB Research Co., Edina, MN; see the Supporting Information).

Approximately 5 g samples of the hydrated and the dehydrated zeolites were loaded into vanadium cans, and diffraction patterns were collected between 10 K and 300 K on the POWGEN beamline[21] at the Spallation Neutron Source at Oak Ridge National Laboratory. Data were collected using two 1 Å wide wavelength bands centered at 1.066 and 4.797 Å. This produced a refinable dataset between 0.3 and 15 Å, but the data were refined between 0.375 and 11.5 Å owing to the lack of discernable reflections outside this region. The possible magnetic space groups for the 300 K $Pm\bar{3}m$ nuclear structure of the dehydrated phase were refined in turn against the data using TOPAS.[22] Consistency with the magnetization and Mössbauer results led to the use of some constraints on the relative magnitudes of moments in the sublattices but these did not degrade the residuals in the final overall fit.

Acknowledgements

Financial support for this work was provided by the National Science Foundation (DMR-1301757) and is gratefully acknowledged. A portion of this research used resources at the Spallation Neutron Source, a DOE Office of Science User Facility operated by Oak Ridge National Laboratory. Use of the Advanced Photon Source at Argonne National Laboratory was supported by the U.S. Department of Energy, Office of Science, Office of Basic Energy Sciences (DE-AC02-06CH11357). Part of this work was performed at the National High Magnetic Field Laboratory (NHMFL), which is supported by the NSF (DMR-1157490) and the State of Florida. S.A.S. is an NHMFL Jack E. Crow postdoctoral fellow. The Mössbauer instrument was funded by the UCGP project 5064 (AO). P.S.W. thanks Dr. Ovidiu Garlea (SNS, ORNL) for discussions regarding the magnetic structure determination.

Keywords: crystal growth · Mössbauer spectroscopy · neutron diffraction · sodalite structure · zeolites

How to cite: *Angew. Chem. Int. Ed.* **2016**, *55*, 13195–13199
Angew. Chem. **2016**, *128*, 13389–13393

[1] E. M. Flanigen, R. W. Broach, S. T. Wilson in *Zeolites in Industrial Separation and Catalysis* (Ed.: S. Kulprathipanja), Wiley-VCH, Weinheim, **2010**, Chapter 1.
[2] M. E. Davis, R. F. Lobo, *Chem. Mater.* **1992**, *4*, 756.
[3] J. Cejka, A. Corma, S. Zones, *Zeolites and Catalysis: Synthesis, Reactions and Applications*, Wiley-VCH, Weinheim, **2010**.
[4] B. Sels, L. Kustov, *Zeolites and Zeolite-like Materials*, Elsevier, Amsterdam, **2016**.
[5] T. Moteki, R. F. Lobo, *Chem. Mater.* **2016**, *28*, 638.
[6] R. B. Borade, *Zeolites* **1987**, *7*, 398.
[7] L. A. Villaescusa, M. A. Camblor, *Chem. Mater.* **2016**, *28*, 3090.
[8] C. S. Cundy, P. A. Cox, *Chem. Rev.* **2003**, *103*, 663.
[9] D. E. Bugaris, M. D. Smith, H.-C. zur Loye, *Inorg. Chem.* **2013**, *52*, 3836.
[10] D. E. Bugaris, H.-C. zur Loye, *Angew. Chem. Int. Ed.* **2012**, *51*, 3780; *Angew. Chem.* **2012**, *124*, 3844.
[11] W. M. Chance, D. E. Bugaris, A. S. Sefat, H.-C. zur Loye, *Inorg. Chem.* **2013**, *52*, 11723.
[12] P. Gütlich, E. Bill, A. X. Trautwein, *Mössbauer Spectroscopy and Transition Metal Chemistry*, Springer, Berlin, **2011**.
[13] D. G. Rancourt, J. Y. Ping, *Nucl. Instrum. Methods Phys. Res. Sect. B* **1991**, *58*, 85.
[14] N. N. Greenwood, T. C. Gibb, *Mössbauer Spectroscopy*, Chapman and Hall Ltd., London, **1971**.
[15] G. P. Gupta, D. P. E. Dickinson, C. E. Johnson, *J. Phys. C* **1978**, *11*, 215.
[16] L. A. Prelorendjos, PhD Thesis, University of Liverpool, **1980**.
[17] D. P. E. Dickson, F. J. Berry, *Mössbauer Spectroscopy*, Cambridge University Press, London, **1986**.
[18] APEX2. "Apex2 Version 2014.9-0", Saint + Version 8.34a and SADABS Version 2014/4. Bruker Analytical X-ray Systems, Inc., Madison, Wisconsin, USA, **2014**..
[19] G. M. Sheldrick, *Acta. Crystallogr. Sect. A* **2008**, *64*, 112.
[20] C. B. Hübschle, G. M. Sheldrick, B. J. Bittrich, *J. Appl. Crystallogr.* **2011**, *44*, 1281.
[21] A. Huq, J. P. Hodges, O. Gourdon, L. Heroux, *Z. Kristallogr. Suppl.* **2011**, *1*, 127.
[22] TOPAS. Version 6. Coehlo Software, Bisbane, Australia.
[23] R. J. Argauer, G. R. Landolt (Mobil Oil Corp), U.S. Patent 3702886, **1972**.

Received: August 10, 2016
Published online: September 21, 2016

